THERMAL-VACUUM TESTING OF A HYBRID ADDITIVE MANUFACTURED PRESSURE VESSEL FOR BROAD AREA COOLING

Lauren R. Gronich, Ama R. Carney, Dr. Alex R. Walker, and Tony F. Skaff

Sierra Lobo, Inc.

Milan Ohio

ABSTRACT

A test campaign is completed to determine the success of a novel hybrid additive manufactured pressure vessel for broad area cooling. The purpose of this pressure vessel is to induce liquefaction of liquid cryogenic propellant internal to the tank, while flowing chilled fluid through tank-integrated channels in a circulated loop. The tests show successful liquefaction at a rate of 0.096 g/s, which is roughly half of the predicted value of 0.2 g/s. Through an analysis of the test results, it is determined that unpredicted heat leak is the cause of the decrease in liquefaction efficiency.

INTRODUCTION

Long term storage of cryogenic fluids is an area of active research for advancing the development and maturation of systems for exploration of deep space by crewed and robotic missions. In Situ Resource Utilization (ISRU), which aims to produce consumable resources such as propellants and water, is one such area of active work. ISRU has the potential to greatly reduce the necessary initial size and mass of exploration systems, reducing overall system complexity, including propulsion system and launch vehicle capability. A number of concepts exist for generating ISRU consumables, one of the most popular being Broad Area Cooling (BAC) tanks which use active cooling via a cryocooler to liquify fluid. To this end, a BAC storage tank leveraging innovative Hybrid Additively-manufactured Tank-integrated Channels (HATCHBAC) is developed.

Traditional manufacturing methods for a tank utilizing BAC requires cooling tubes to either be attached to the outside walls of the tank or to be placed on structures secured to the inside of the tank. To reduce overall complexity of the manufacturing process cooling channels are printed directly into the walls of the cryogenic storage tank as it is being built. A thorough thermal-fluid analysis of the design of this novel HATCHBAC architecture has been discussed previously.

A testing campaign is completed to validate and assess the ability of the proposed design to maintain the liquefaction rates necessary for the long-term in-situ storage of cryogenic fluids. This campaign includes three verification and validation tests of individual system components as well as nine tests of the fully assembled system. These tests are aimed at validating expected liquefaction rates and heat leak against previous modeling efforts. For these tests gaseous nitrogen is condensed withing the tank via cold helium pushed through a cooling loop. The cooling loop contains a circulator, the BAC channels, and a heat exchanger positioned between a 60 W cryocooler and a heater, which is used for helium temperature control.

Figure 1: Interior machining of the cryogenic tank during early stages of production[1].

BACKGROUND

The goal of testing the HATCHBAC tank was to verify that the tank will condense and liquify gaseous fluid held internal to the tank. With this requirement, two independent systems handling two different fluids were designed to produce a test set up that are efficient and effective. The condensed fluid internal to the HATCHBAC tank was nitrogen, and the cooling agent to flow through the BAC channels was helium.

To preserve the helium, a cooling loop was developed to circulate the helium through the BAC channels, and back through a heat exchanger attached to the coldhead of a cryocooler. The helium temperature was to stay below the saturation point of nitrogen inside the tank to ensure effective nitrogen liquefaction. To measure the liquefaction rate, nitrogen was slowly allowed into the tank such that the pressure in the tank stayed constant. With constant pressure the mass flow rate of vapor into the tank is the liquefaction rate, thus conceptually completing both nitrogen and helium systems for the condensation thermal vacuum testing.

TEST DESIGN

Instrumentation Layout

The P&ID of the full test setup is shown in **Figure 2**. To fully characterize the thermal phenomena occurring within the test, a series of temperature and pressure sensors were installed at various points throughout the system. This section will detail the instrumentation in the test setup.

Circulation Loop

Instrumentation for the helium inlet started with pressure gauge PG 3224, which measured helium supply tank pressure, followed by pressure regulator PCV 3225, which regulated helium tank pressure from 2500 psig to 85 psig. This was then followed by HV 3207 which controlled helium flow into the circulation loop. Three vent lines were installed in the helium inlet system. The first was regulated by HV 3226. The second, which was placed after HV 3207, contained the pressure gauge for the line (PG 3227) followed by vent valve HV 3219. The third was the line containing the relief valve (PSV 3210). Upon entering the vacuum chamber, a pressure transducer (PT 3209) read and recorded the pressure within the helium line.

After the tee to the helium supply line is the low end of the circulator pressure differential measurement (PDT 3220), followed by the circulator (H 3212), and then the high end of PDT 3220. Next the temperature before the heat exchanger is measure by diode TE 3214, followed by the heat exchanger (H3200), and then the temperature after the heat exchanger (TE 3215). The helium then flows through the channels within the

[1] Image credit: Big Metal Additive (2023).

BAC tank (N 4200). Helium temperature after the tank is measured by TE 3217 and the circulation loop is complete.

Heat Exchanger

The heat exchanger layout consists of a G10 plate (H 3202), a trim heater (H 3201), the heat exchanger (H 3200), and the coldhead of the cryocooler (H 3101). The heater is secured to the heat exchanger and the G10 plate fastens directly to the coldhead, ensuring good thermal contact between the heater and the heat exchanger. Two thermocouples, TC 3221 and TC 3205, monitor the trim heater temperature to ensure it doesn't overheat. Diode TE 3204 measures the heat exchanger temperature and diode TE 32023 measures the cold head temperature.

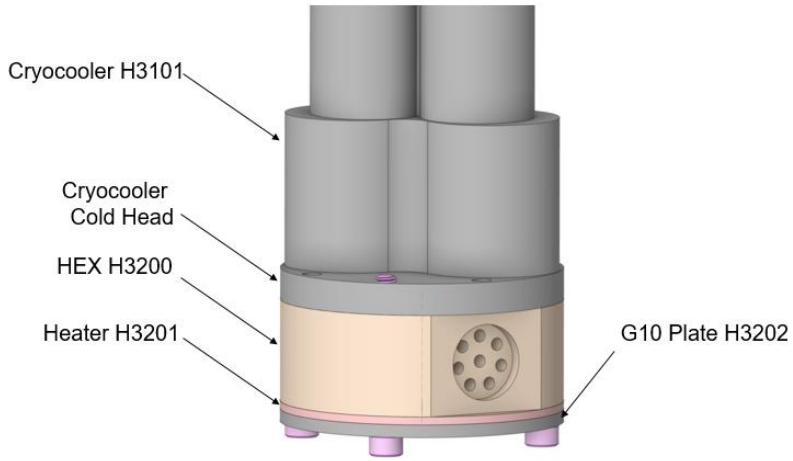

Figure 3: The cooling loop hot-side heat exchanger was mounted directly to the cryocooler head with thermal grease between the two surfaces. On the other side of the heat exchanger, an electric heater was attached via epoxy, and a G10 plate provided extra support to keep the heater in contact with the heat exchanger.

Liquid Inlet

Liquid nitrogen is added to the tank to prechill the tank wall during thermal testing. Valve HV 4201 controls liquid inlet into the system. The line then splits into the drain arm and the dip tube. Drain valve HV 4202 remains shut during liquid fill. Once the tank is at the desired liquid level, it is then opened to allow liquid to drain from the tank. If the drain is not open LN_2 flows down the dip tube and into the tank.

Gas Inlet

Gas is added into the tank during nominal test operation via a 12 pack of GN_2. Pressure on the 12 pack is monitored by PT 4240 and flow out is controlled by HV 4239. Immediately exiting the 12 pack, the pressure is regulated from 2500 psig to 85 psig by PCV 4203, which is followed by relief valve PSV 4205 set at 100 psig. After the relief valve is flow meter FM 4204 and pressure transducer PT 4242. The pressure is then controlled by PCV 4229 from 85 psig to the test pressure, nominally 10 psig. PG 4231 is used by a local operator to verify the downstream pressure after PCV 4229.

Next, the flow path splits into the vent and inlet systems. In the inlet line are the two flow control valves HV 4206 and HV 4227 plumbed in parallel. They connect to the dip tube in the tank. On the dip tube inlet path is the high end of pressure differential measurement PDT 4208 which measures tank liquid level as a

function of increasing liquid head pressure. A tee in the line leading out of the tank to the vent system splits flow between another drain valve (HV 4222), the low end of PDT 4208, and the actual vent components. HV 4228 protects the differential pressure transducer PDT 4208 during purging, initial chilldown, and drain operations. Pressure transducer PT 4210, plumbed in near the low end of PDT 4208, measures tank pressure. Relief valve PSV 4214, set at 100 psig, protects the tank from overpressure. HV 4212 is used to vent the tank to atmospheric pressure. PCV 4213 is used to help keep the tank pressure above atmospheric pressure, and check valve CV 4230 prevents backflow into the system.

Tank Wall

Several temperature sensors on the tank wall help determine heat transfer throughout the system and help identify any hotspots that exist. Two diodes, one placed on top of the tank (TE 4220) and one placed on the bottom of the tank (TE 4221), are used to measure the temperature differential between the top and bottom of the tank. A circumferential ring of thermocouples was placed around the tank (TC 4216 – 4219) to identify any hotspots that might occur between cooling channels. In addition, TC 4223 and TC 4224 measure the vertical temperature gradient and align with TC 4216. All temperature elements, except thermocouple TC 4225, were directly attached to the tank wall using Stycast 2850FT. TC 4225 was attached to the outer layer of the tank's MLI blanket with an adhesive patch (as purchased with the thermocouple) and was directly aligned with TE 4221 to determine temperature differential across the MLI.

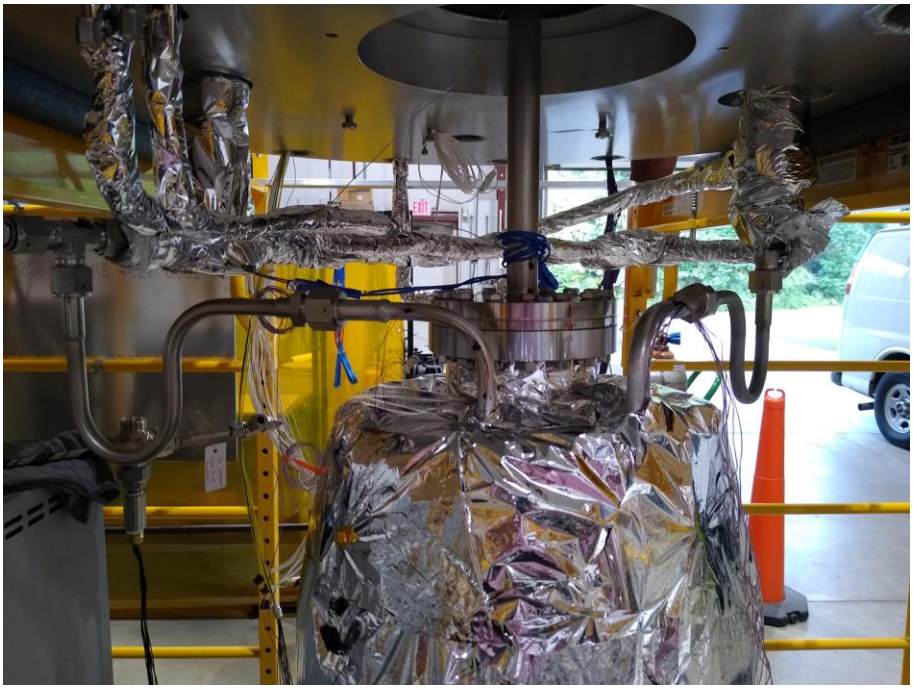

Figure 4. The broad area cooling tank was suspended from the lid of Sierra Lobo's VC-3 vacuum chamber, connected to a cooling loop, and fully insulated for thermal-vacuum testing.

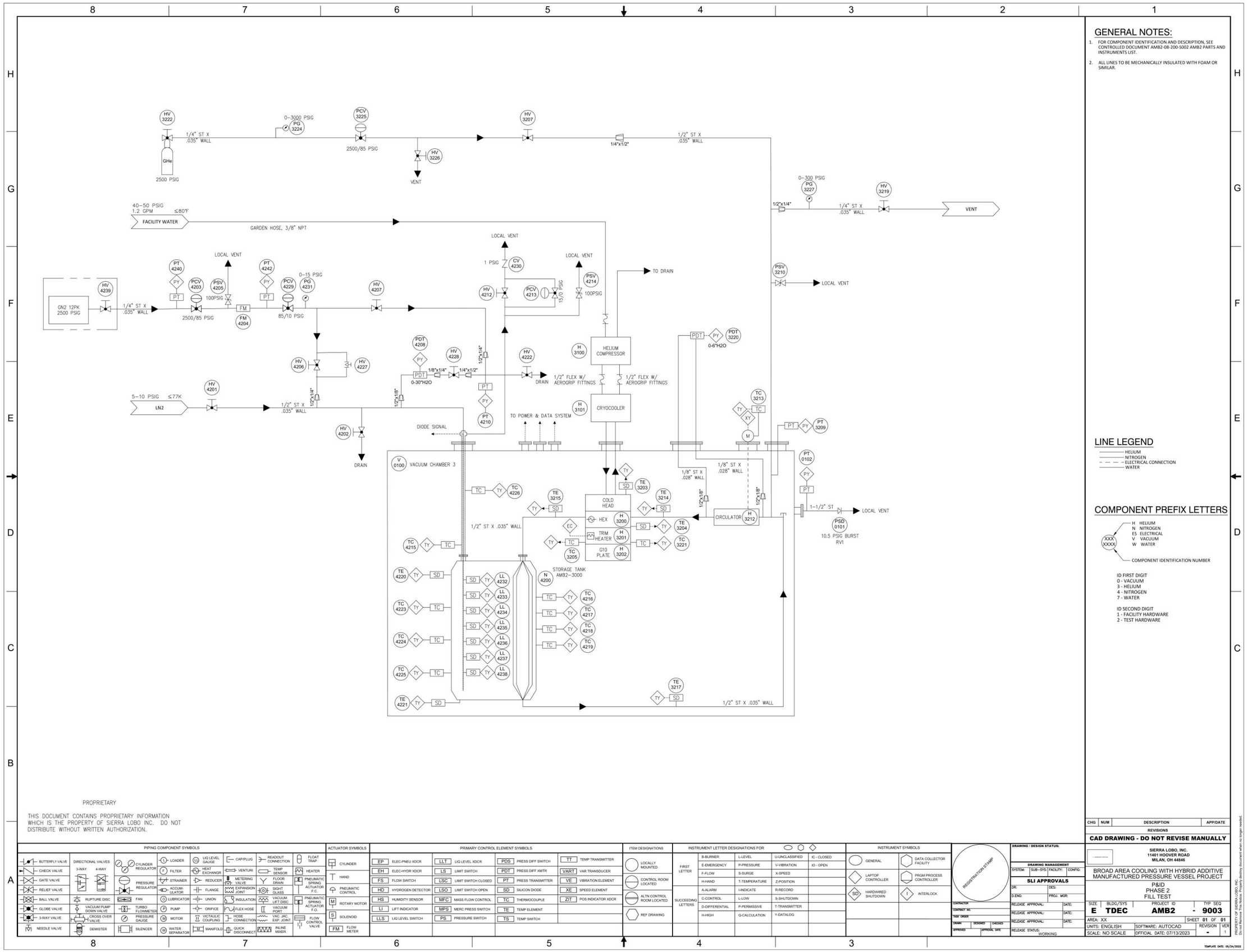

Figure 2: Broad area cooling tank thermal-vacuum test piping and instrumentation diagram (P&ID).

INITIAL TESTING RESULTS

After the completion of the preliminary analysis, design, and fabrication by Big Metal Additive (BMA), a series of structural and Independent Verification and Validation (IV&V) tests are developed to ensure the efficacy and safety of the components used in the main thermal vacuum testing campaign.

Structural Tests

Cold Shock Test

The cold shock test was conducted by filling the tank approximately half-full of liquid nitrogen and rotating the tank along its longitudinal (normally vertical) axis to coat the interior with liquid nitrogen, thereby cooling all metal mass to liquid nitrogen temperatures.

Figure 5: The broad area cooling tank cold shock test performed outside of Sierra Lobo's shop.

Proof Pressure Test

Pressure tests were done for both the broad area cooling tubes and tank. The tubes were pressurized in 10% increments increments up to the maximum pressure of 94 psig using room temperature gaseous nitrogen. At each increment, the tubes were held at that condition for 5 minutes before moving to the next pressure. A maximum pressure was held for 15 minutes before completing the tube pressure test. The tank was also pressurized in 10% increments up to the maximum 128 psig with room temperature water. Similarly, each increment was held for 5 minutes, with the maximum pressure being held for 15 minutes.

Helium Mass Spectrometry Leak Test

The helium mass spectrometry leak test was done on the broad area cooling tubing and tank. Two leaks were found in the tubing between 10^{-6} and 10^{-7} $Pa \cdot m^3 \cdot s^{-1}$. After having no evidence of leaks in the tank portion, the two tubing leaks were welded shut, and the tank was once again cold shocked and proof pressure tested.

Figure 6: Small pinhole leaks in the BAC channels were located during helium mass spectrometry testing.

Thermal IV&V Tests

Cryocooler Performance Verification Test

For the first IV&V test, the cryocooler was operated to verify its performance matched the vendor datasheet. Results for this test are shown in **Figure 7** below. The error between the experimental and given temperature data averaged 4.5% when excluding the last data point, the power draw at 60 W. This point can be ignored due to the data acquisition system crashing during the last portion of the test, and ultimately failing to reach steady state. The temperatures were not able to reach steady state due to the data acquisition system crashing during the last portion of the test.

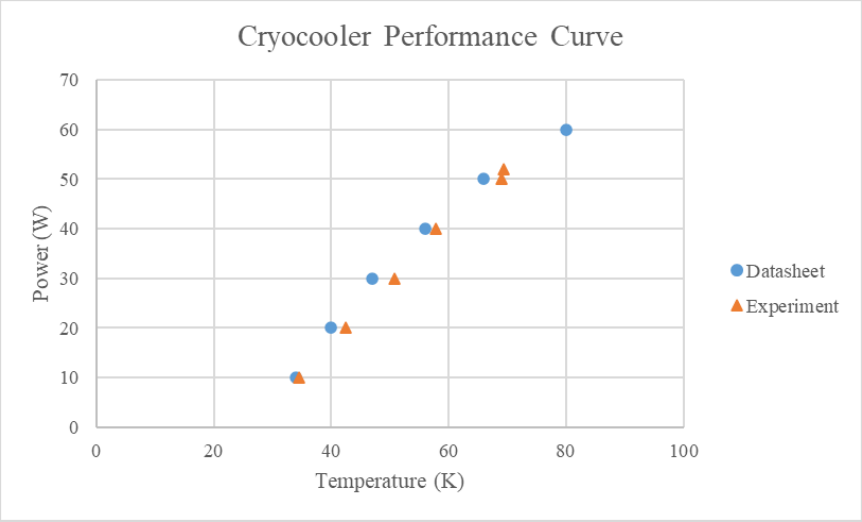

Figure 7: Results of the first IV&V test show that PT-60 cryocooler performance reported on the datasheet agrees well with the measured heat load as a function of cryocooler head temperature.

Heat Exchanger and Orifice Performance IV&V Test

The second IV&V test was intended to verify that performance of the heat exchanger agreed reasonably well with the predictive Thermal Desktop models and to verify and validate use of a custom-machined orifice to estimate cooling loop mass flow rate in the final IV&V test.

During this test, instrumentation issues arose, making it difficult to get any heat exchanger validation information. Due to the nature of the heat exchanger not interfering with the accuracy of the circulator performance readings and allowing for all necessary instrumentation to remain within the system, verification and validation for the heat exchanger was moved to be completed after the third IV&V test. Despite not initially being able to get data for the heat exchanger, the orifice was still able to be validated against a Thermal Desktop model. The test for the orifice was done with room temperature, 85 psig nitrogen. The PDT N3208 recorded the change in pressure across the orifice as the flow reached steady state after incremental flow rate increases, as shown in **Figure 8**.

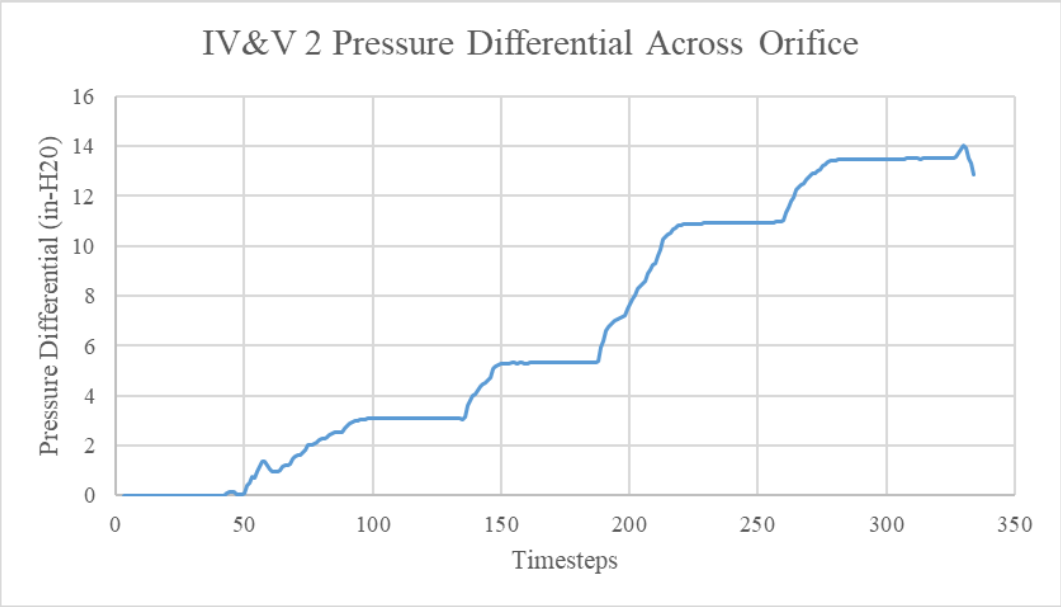

Figure 8: Pressure differential measurements across the orifice machined for the second IV&V test provided a calibration curve which was used for the third IV&V test.

With the pressure differential recorded, and the flow rate being tracked from the flowmeter, it became possible to validate the orifice. Due to the orifice being machined imprecisely using a drill bit, it was evident that the Thermal Desktop model would not completely reflect the test results. However, the Thermal Desktop model was able to be altered with some iteration until the results matched and could be translated to an equivalent pressure drop for the eventual helium that would pass through the line. In **Figure 9**, the unaltered Thermal Desktop model results for pressure drop was plotted against the test pressure drops at equivalent flow rates.

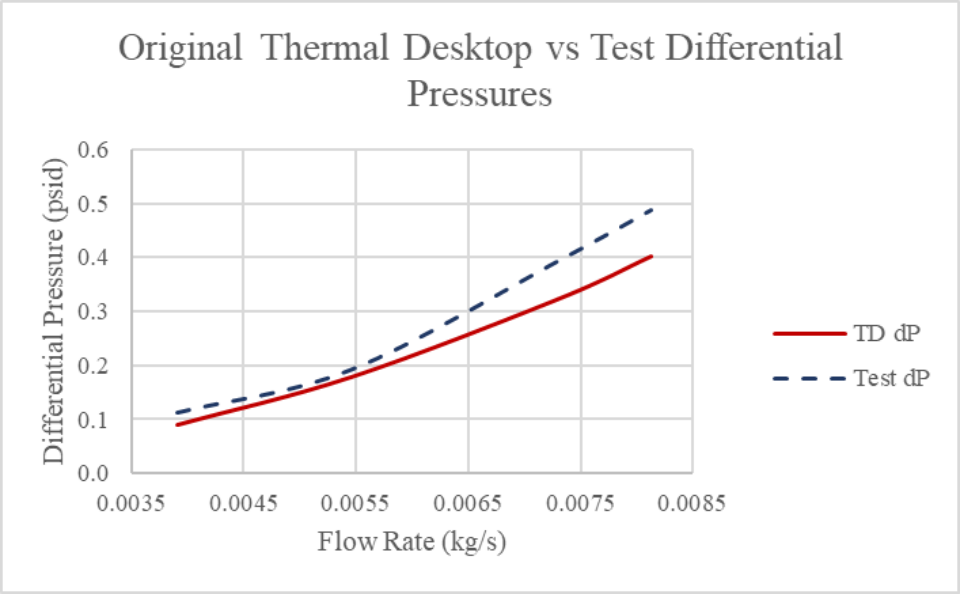

Figure 9: Initial orifice differential pressure predictions as a function of flow rate made using the Thermal Desktop model did not match the data well.

It was observed that the error in the first set of data averaged 22%. While 22% is large, the error was consistent throughout each data point, indicating that the initial size of the orifice was incorrect in the original Thermal Desktop model. Next, as mentioned, the Thermal Desktop model was altered to better fit the test data.

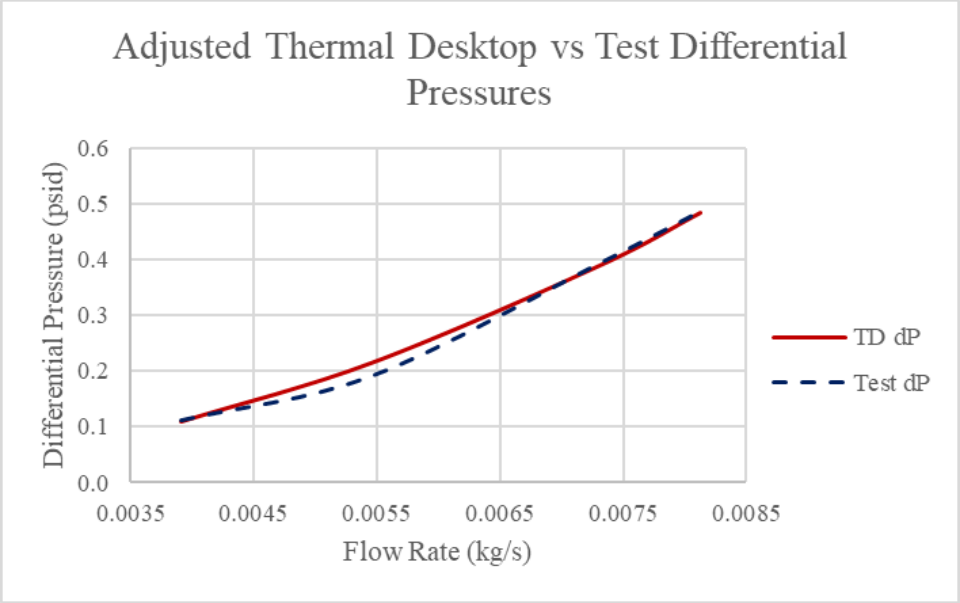

Figure 10: A corrected Thermal Desktop model provided orifice differential pressure predictions as a function of flow rate much closer to those measured during the second IV&V test.

After adjusting the orifice diameter, the Thermal Desktop results fit closely to the test data, averaging a 1% error between the values, and comfortably verifying the orifice for the circulator performance IV&V test, as shown in **Figure 10**.

In addition to the orifice being validated, the heat exchanger also needed to be validated. Thermal Desktop models were used to validate the temperatures seen across the surface of the heat exchanger as well as upstream and downstream of the heat exchanger. Giving the model the same inputs the IV&V test produced, the model results mimicked almost exactly the test data, successfully verifying and validating the design and construction of the heat exchanger.

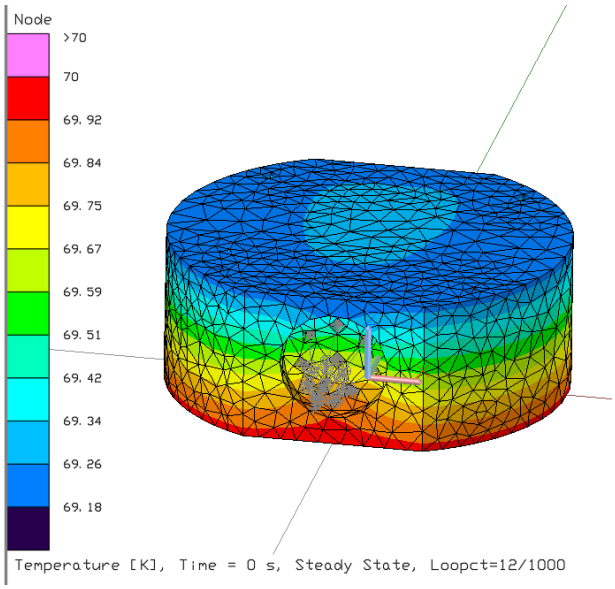

Figure 11: Heat exchanger surface temperature was validated using Thermal Desktop.

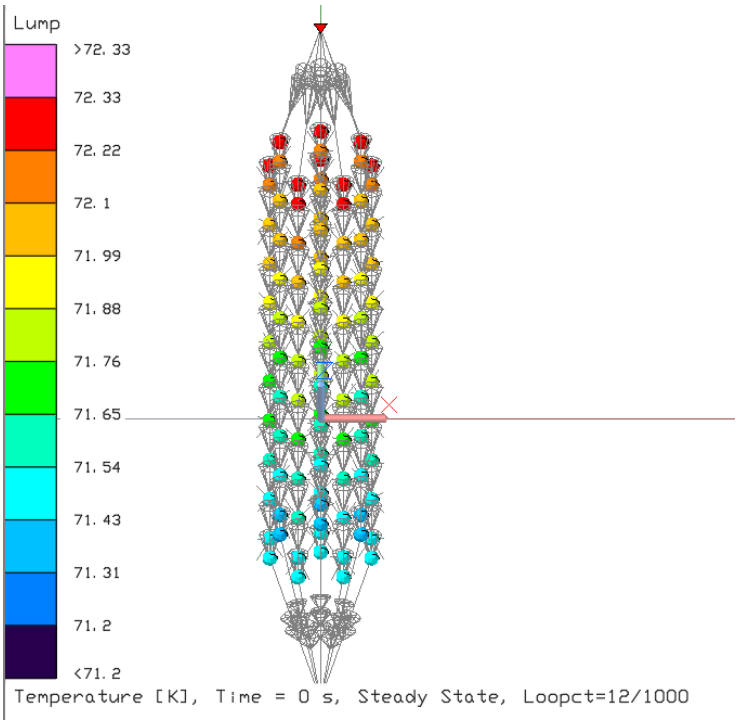

Figure 12: Heat exchanger fluid temperature was validated using Thermal Desktop.

Circulator Performance IV&V Test

The last IV&V test verified circulator functionality and validated the heat exchanger against the Thermal Desktop model. The circulator flow rate was calculated using vendor provided equations, finding the flow rate from the cooling loop static pressure, cooling loop total pressure drop, circulator rotational speed, and cooling loop helium temperature.

This result was compared to the flow rate estimated using the predictive orifice flow rate models created in the second IV&V test, corrected for use in helium as shown in **Figure 13**. Comparison of flow rates predicted using the vendor equations and flow rates predicted using the orifice models for all circulator rotational speeds achieved during testing is shown below in **Figure 14**.

The flow rate prediction using the circulator state equations is, on average, about 14% lower than the flow rate prediction using the orifice, as shown in **Figure 14.** However, the uncertainty bounds of the estimate made using the circulator state equations lie almost completely within the uncertainty bounds of the estimate made using the orifice, so the two estimates agree, within the bounds of their respective uncertainties. Because the uncertainty of the orifice estimate is about three times that of the circulator state estimate, the flow rate measurement from the circulator state equations was used for the final thermal-vacuum test.

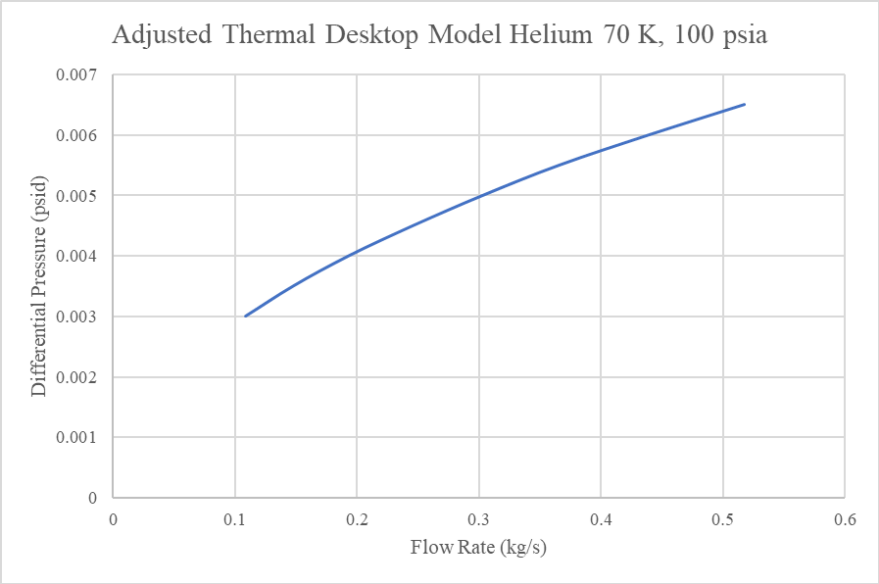

Figure 13: The Thermal Desktop model generated in the second IV&V test was corrected for use in helium at 70 K and 100 psia to yield a relation between pressure drop over the orifice and estimated cooling loop flow rate.

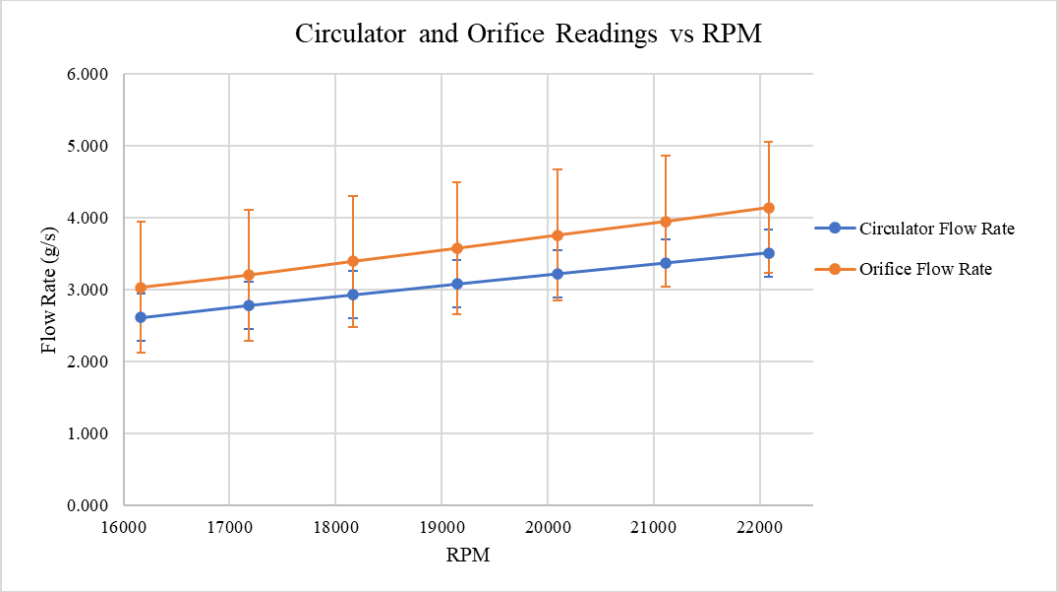

Figure 14: Comparison of the flow rate measured using the custom-made orifice calibrated in the second IV&V against the flow rate measured using the circulator flow rate prediction equation shows agreement within the estimated bounds of uncertainty.

THERMAL TEST RESULTS

Condensation Fill Tests

The goal of condensation fill testing was to verify the HATCHBAC tank was able to condense gaseous nitrogen into liquid consistent with condensation analysis, thereby validating predictive models used for HACHBAC tank design. Several fill tests were performed to gather enough data to validate thermal-fluid models.

The first condensation test started with the tank filled with gaseous nitrogen and tank walls pre-chilled to cryogenic temperatures. Nitrogen gas was fed into the tank and condensed to a liquid until the tank was full. **Figure 15** shows the liquid height over the duration of the test. In this plot, two different liquid level measurement methods have been recorded and compared. The first method used the pressure differential gauge PDT 4208, shown in a solid black line. The second method used silicon diodes LL 4232 through LL 4238, placed evenly along the dip tube inserted into the tank.

Condensation rate was found using three different measurement techniques. 1) A pressure differential measurement between tank ullage and the bottom of the tank, 2) A series of seven diodes along the dip tube, and 3) the mass flow rate into the tank. The slope of the dP measurement in **Figure 15** corresponds to a liquefaction rate of about 4.2 inches nitrogen per day. Over the linear portion of this data, the tank is a cylinder with outer diameter of 14 inches and wall thickness of about 0.1 inches. Therefore, liquefaction rate was about 628 in^3 (10.29 liters) of nitrogen per day. Using the density of liquid nitrogen at 1 atm and 77 K, 0.807 kg/l, this amounts to 8.3 kg of nitrogen per day, or a 0.096 g/s liquefaction rate.

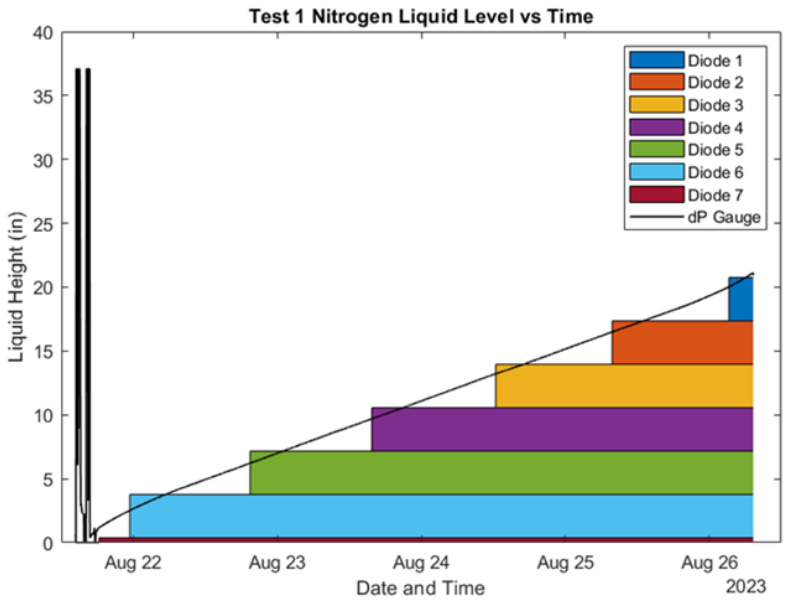

Figure 15: Liquid level accumulation for the first condensation test.

During condensation tests, the condensation rate was also taken to equal the mass flow rate of gaseous nitrogen into the test article, because the vent was closed. To keep tank pressure constant as gaseous nitrogen in the tank condensed into liquid, gaseous nitrogen was slowly supplied to the tank via the dip tube. Because of the great density disparity between the liquid and gaseous nitrogen, almost an equal amount of gaseous nitrogen was needed from the supply to replace the volume of gaseous nitrogen being condensed into liquid. Therefore, the condensation rate is nearly equal to the flow rate into the system. Mass flow rate of gaseous nitrogen into the tank during the first condensation test is shown below in **Figure 16**. On average, this mass flow rate was slightly less than 0.1 g/s, which is consistent with the 0.096 g/s liquefaction rate estimate found using the dP and diode sensors.

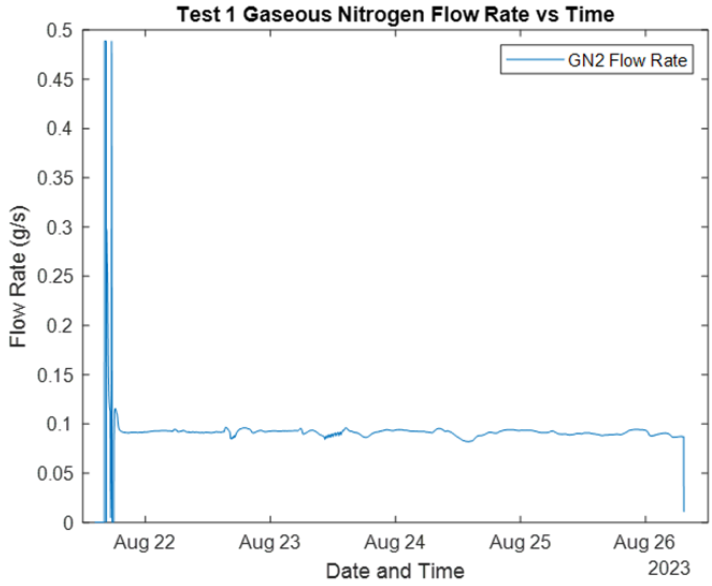

Figure 16: Nitrogen flow rate into test tank for the first condensation test.

It was noted that the condensation rate was only half of the expected rate of 0.2 g/s. Helium temperatures throughout the cooling loop system, shown below in **Figure 17**, were also noted to be about 8 K higher than predicted.

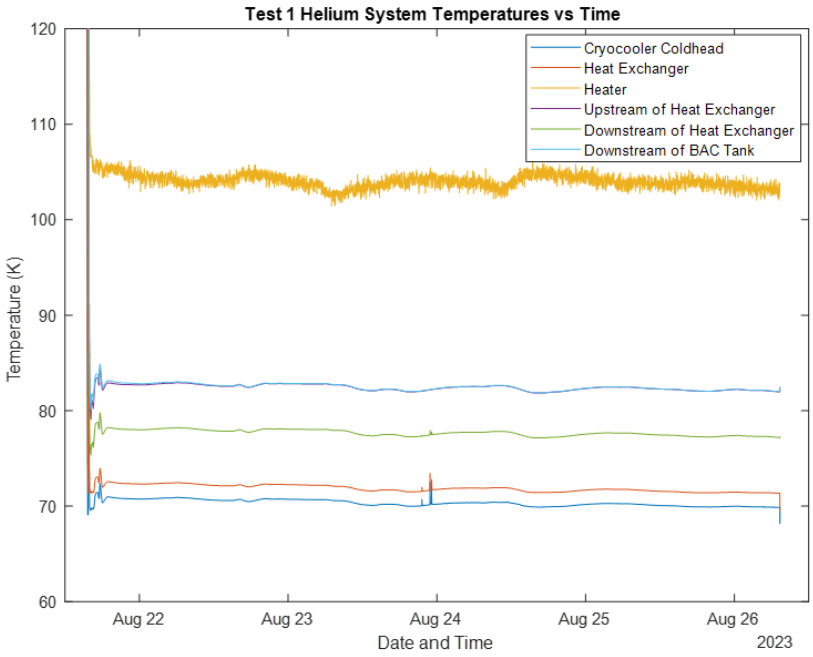

Figure 17: Helium system temperatures during the first condensation test.

Higher than expected cooling loop temperatures indicate the cooling loop was operating at a lower-than-expected efficiency. **Figure 18** shows the helium temperatures across the heat exchanger (temperature diodes TE 3214 and TE 3215). Lift from the cryocooler was calculated to be 46.7 W using these temperature values, the helium pressure taken from pressure transducer PT 3209, and the flow rate calculated from differential pressure gauge PDT 3220, shown in **Figure 19**. This value is below the 60 W lift for which the cooling loop system was designed but could be attributed to the decreased efficiency of operating in a different temperature range and at a different flow rate than originally calculated.

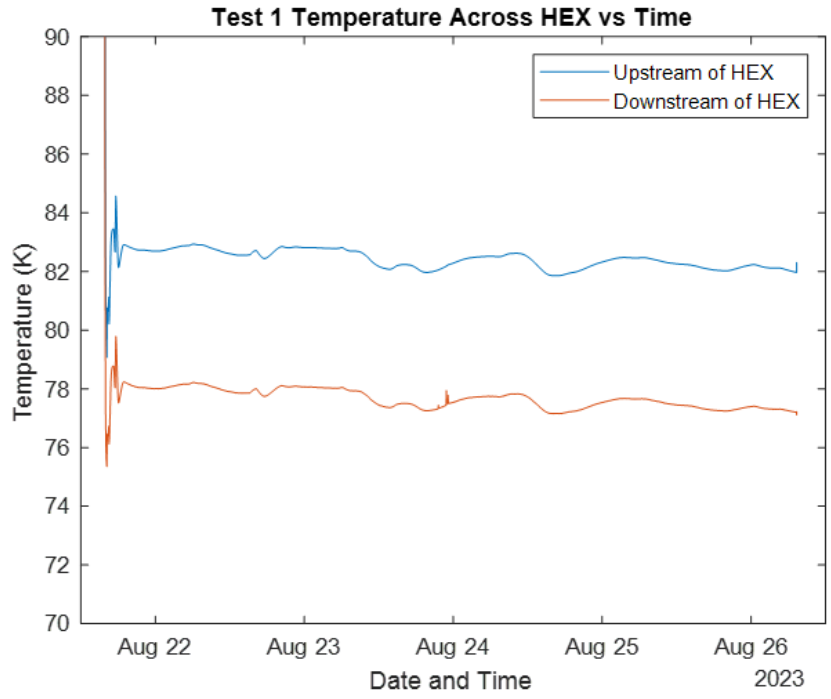

Figure 18: Helium temperatures upstream and downstream of the heat exchanger during the first condensation test.

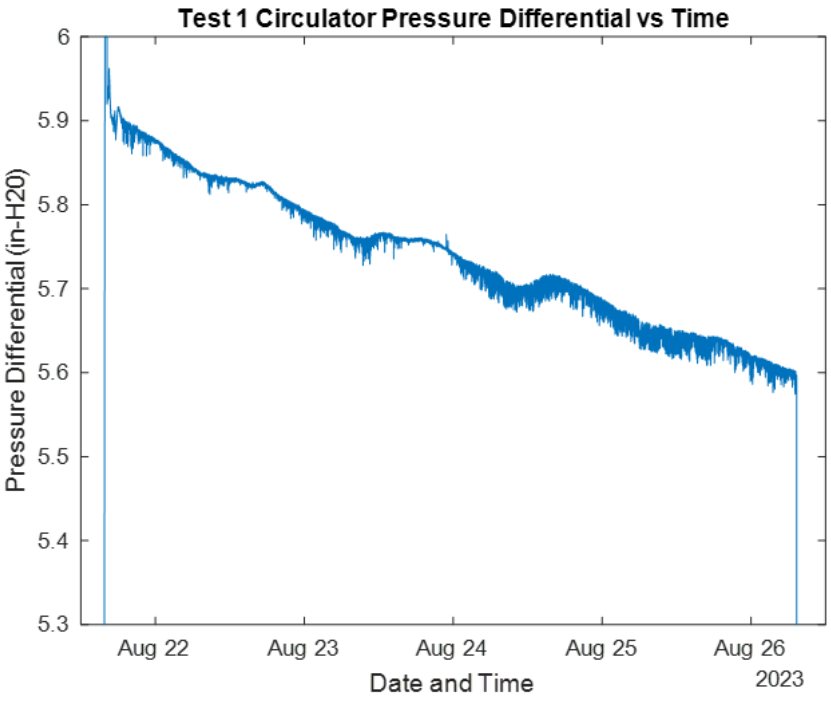

Figure 19: Pressure differential across cooling loop circulator (used to calculate helium flow rate) during first condensation test.

Lift across the BAC tank was found to be 47.1 W, calculated from the cooling loop flow rate and enthalpy change of the cooling loop helium between the inlet and outlet of the BAC channels. Cooling loop flow rate was found using the differential pressure across the circulator (PDT 3220) with vendor provided equations. Enthalpy of the helium was found using REFPROP with measurements from temperature diodes TE 3215 and TE 3217 and pressure transducer PT 3209. In previous analyses, the total heat transfer throughout the system can be broken up into three categories, the heat transfer across the heat exchanger, the heat transfer across the BAC tank, and the heat transfer to the whole system due to various sources of heat leak.

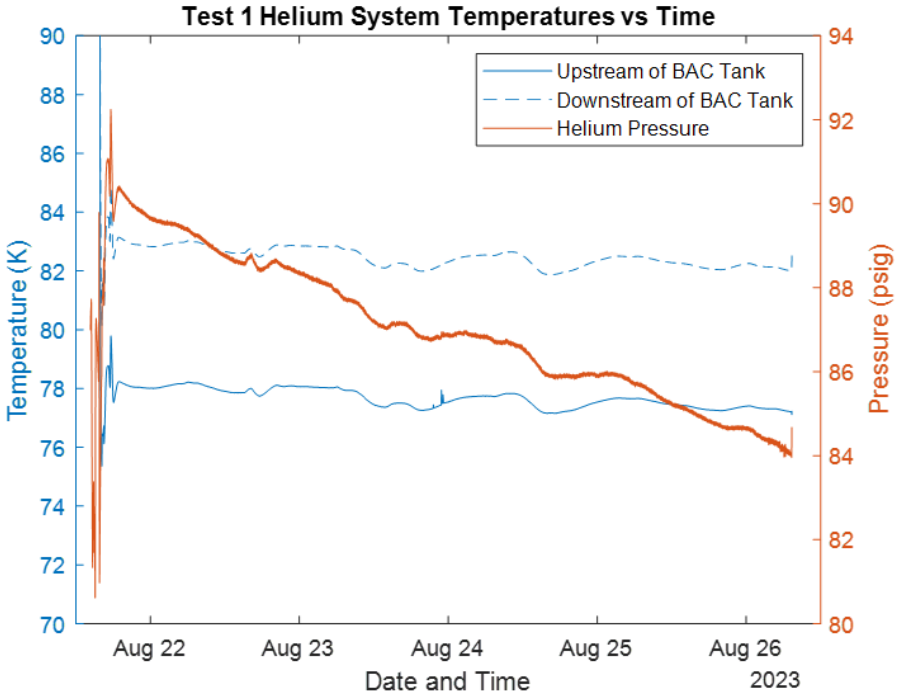

Figure 20: Helium conditions upstream and downstream of the test article during the first condensation test.

Tank pressure stayed relatively constant during the first condensation test, wavering with the temperature difference of the ambient test surroundings, as shown in **Figure 20**. Tank temperatures also wavered within the span of a day, with the bottom of the tank reading slightly below the saturation temperature of nitrogen at the corresponding tank pressure, and the top of the tank reading slightly above the saturation temperature of nitrogen, indicating that the vapor remained superheated to some extent. The overall temperature curves trended downward over time, which can be attributed to the added nitrogen vapor cooling more as it traveled through the dip tube and through the accumulated liquid as it increased in depth.

These results indicate more heat entered the system than was previously expected, impacting the temperature difference between the walls of the tank and the nitrogen inside of the tank, ultimately decreasing the condensation rate in the tank.

To obtain more data on heat leak, a boil-off test was run. Starting with the liquid accumulated in the tank from the second condensation test, the cryocooler and cooling loop were turned off, and the tank was allowed to sit for an extended period, causing some of the liquid nitrogen to boil off. As with the

condensation test data, heat leak into the system was estimated using an energy balance calculation, The tank pressure was recorded using PT 4210, and the top and bottom of the tank's temperature were recorded using TE 4220 and TE 4221, shown below in **Figure 22**. Heat leak estimated using these quantities and the energy balance relation is shown below in **Figure 23**.

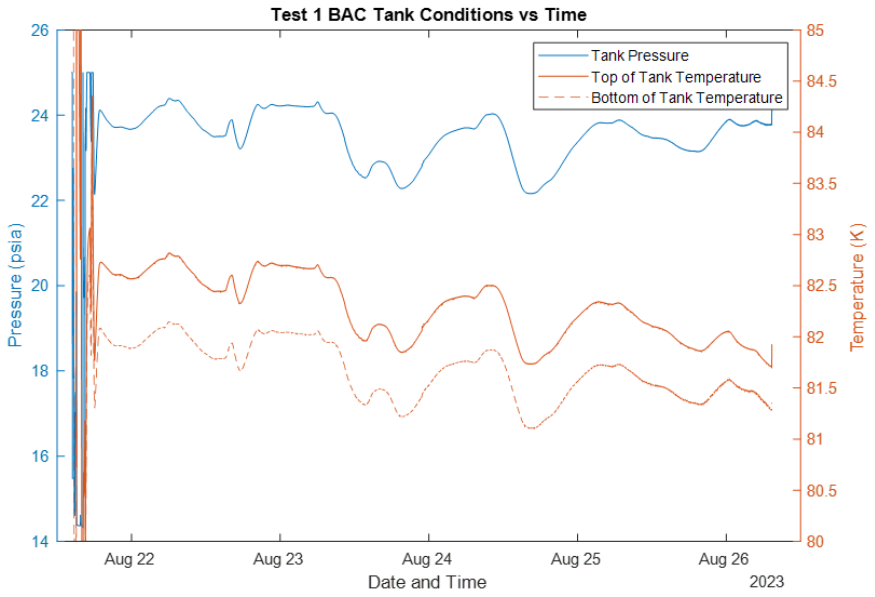

Figure 21: Tank temperature and pressure during the first condensation test.

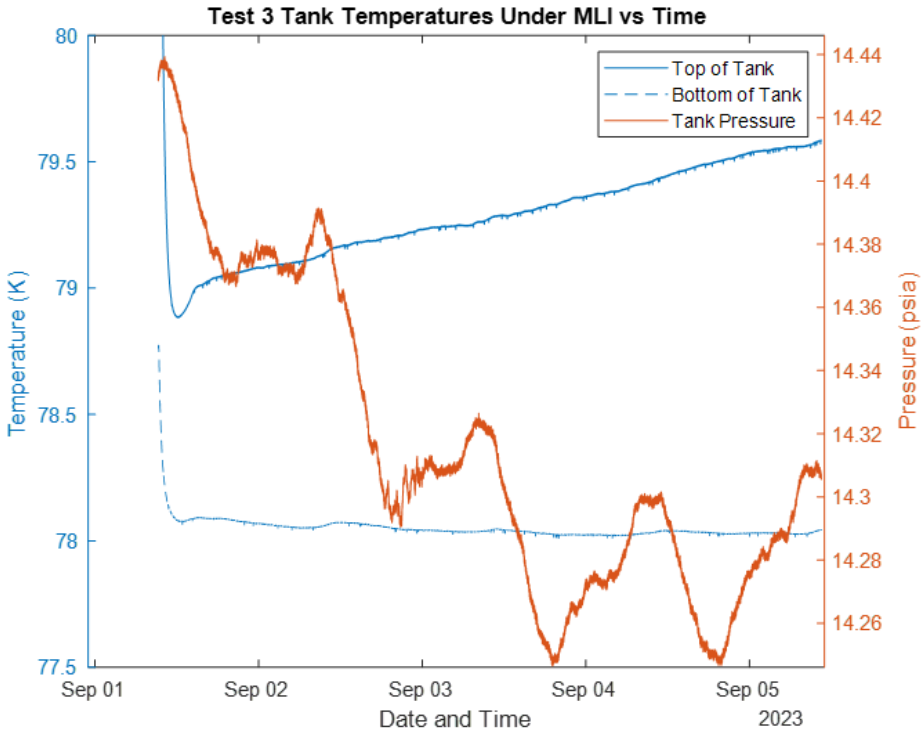

Figure 22: Internal tank conditions during boil-off test.

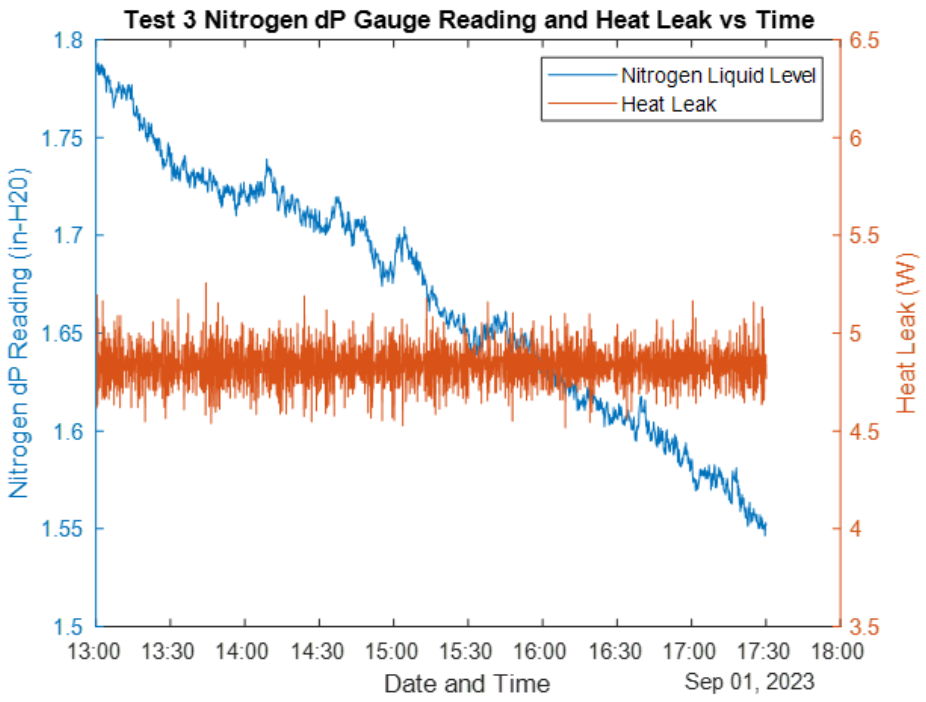

Figure 23: Nitrogen liquid level and heat leak during initial part of boil-off test.

As shown above, the heat leak into the liquid averaged 4.8 W during the boil-off test, but it is important to note some inherent flaws of assuming this to be the total heat leak into the system. This calculated heat leak is only the direct result of vaporization of liquid nitrogen. The heat leak does not account for any bulk heating of the liquid or vapor in the tank. It is particularly important to note that the liquid surface area in contact with the tank wall is far less than the vapor surface area in contact with the tank wall. In addition, as assumed previously, most of the heat leak coming into the tank would be through the flange on the lid of the tank. This, in turn, would disproportionally heat the top of the tank more, and therefore cause the vapor to heat up at a far faster rate than the liquid. Because the vapor temperature was not recorded for any of these tests, it is impossible to tell what the bulk heating to the vapor would be. In addition, there is also still gas remaining in the helium lines within the tank that can absorb heat and vent through the system, also contributing to a lower apparent heat leak, as evidenced by the test data.

Several other tests were run, altering tank pressure, helium flow rate, and fill level to achieve more data points for anchoring the earlier thermal-fluid models, all pointing towards incorrect modeling assumptions in estimated heat leak. These results and comparisons are shown in the section below.

Anchoring Thermal-Fluid Models

Predictions of the models used to design the HATCHBAC system were clearly inconsistent with the heat leak measured during testing. Therefore, it was necessary to modify the initial models in order to anchor them.

Firstly, the anchored value of heat exchanger heat transfer needed to be calculated. Instead of using the original modeled values, the test results were input. This includes the upstream temperature from TE 3214, the downstream temperature from TE 3215, and the helium pressure from PT 3209. The time history of heat exchanger heat transfer was found using the mass flow rate of helium calculated using the circulator flow rate equations and the change in enthalpy of the helium over the heat exchanger. Enthalpy upstream

and downstream of the heat exchanger was found using REFPROP along with the corresponding temperature and pressure measurements. The time history of heat exchanger heat transfer was averaged over the portion of data corresponding to steady-state and taken as the anchored value of heat exchanger heat transfer.

Next, the anchored value of heat transfer across the broad area cooling tank was calculated using a similar method to that used for the heat exchanger. This time, the temperature values upstream and downstream of the tank were taken from TE 3215 and TE 3217, respectively, the pressure was taken from PT 3209, and the helium flow rate was calculated using the circulator vendor provided equations.

Finding the anchored value of heat transfer across the circulator followed the same method as the heat exchanger and broad area cooling tank taking temperatures upstream and downstream of the circulator from TE 3217 and TE 3214, respectively.

The amount of heat going into cooling and condensing nitrogen was calculated from the enthalpy change and heat of vaporization (liquefaction) of the nitrogen as it was added to the BAC tank. The pressure recorded by PT 4210 was taken as the pressure of the nitrogen at each of three different states. The first state was the gaseous nitrogen entering the system at ambient temperature. The second state was saturated nitrogen vapor. And the third state was saturated liquid nitrogen. Heat transfer from the nitrogen from state one to state two was calculated using state one and state two enthalpies and the flow rate recorded from FM 4204. Heat transfer from the nitrogen from state two to state three was calculated using heat of vaporization and the flow rate from FM 4204. The sum of these two values were taken to equal the total heat lifted from the nitrogen to cool and condense it.

Radiation heat leak for the BAC tank was calculated using the basic radiation heat transfer equation.

$$q = \varepsilon\sigma A(T_1^4 - T_2^4) \tag{1}$$

Where ε is the emissivity of the MLI, σ is the Stefan-Boltzmann constant, A is the area over which heat transfer occurs, T_1 is the ambient temperature, and T_2 is the MLI temperature taken from TC 4225 on top of the MLI blanket.

Conduction heat leak along the dip tube was calculated using an average thermal conductivity value for the dip tube material, the geometry of the dip tube, and temperature measurements (TC 4226 and TC 4215) taken at two locations along the height of the dip tube outside of the test article.

The total heat leak from the diodes was assumed to be 0.25 W. This heat leak was assumed to be the dominating heat leak for all instrumentation attached to the system.

Lastly, the heat leak from the flange to the lid of the broad area cooling tank was estimated. This value holds the largest uncertainty, because, without further intensive investigation, the contact resistance between the tank material and bolts holds a high uncertainty. This value was estimated using the *Spacecraft Thermal Control Handbook* but had to be extrapolated from a table following similar material features. For this calculation, a thermal resistance network was created, going through the flange thickness and through the bolts. The temperatures for this calculation were taken to be those from TC 4215 and TE 4220.

It is important to note the uncertainty for all values used to anchor the thermal model. Considering all of the inputs required to do these calculations, the total uncertainty in heat transfer adds up to 26.6 W including the heat exchanger heat transfer, the broad area cooling tank heat transfer, and condensation values. Therefore, so long as any unaccounted-for heat leak errors fall within 26.6 W, the calculations are verified

to the best of the instrumentation abilities, though it still cannot be ruled out that additional factors beyond what was accounted for are contributing to the discrepancy.

The values shown below in **Table 1** account for the total heat transfer found in three different tests. Test 1 was the test run under standard conditions shown in the above section. Test 6 was a high-pressure test, where the internal tank pressure was approximately 45 psia. Test 8 was a top-fill test, with the internal tank pressure being held at about 21 psia.

Table 1: Nitrogen liquid level and heat leak during boil-off test.

Heat Transfer Analysis Validation			
	Test 1 (W)	**Test 6 (W)**	**Test 8 (W)**
Heat Exchanger (±13.140 W)	46.525	80.023	78.996
BAC Tank (±13.140 W)	47.068	79.205	75.844
Nitrogen Cooling and Condensation	38.427	43.781	36.201
Total Heat Leak	20.925	22.985	34.986
Circulator	-0.543	0.818	3.152
Radiation	1.236	0.764	2.371
Dip Tube	0.920	0.875	0.862
Diodes	0.250	0.250	0.250
Flange	19.062	20.278	28.351
Theoretical System Heat Leak	8.641	35.424	39.643
Unaccounted for Heat Leak	12.827	-13.257	-7.809

In the above table, each row denotes a different source of heat leak, as previously explained. The total heat leak comprises the heat leaks from the circulator, radiation, dip tube, diodes, and flange. The theoretical system heat leak is the discrepancy in heat transfer between the helium to the nitrogen across the broad area cooling tank. Therefore, the unaccounted-for heat leak is either the over- or underprediction of heat leak into the system.

Again, as shown in **Table 1**, all unaccounted-for heat leak values fall within the uncertainty of the instrumentation used for the BAC system thermal-vacuum testing, and therefore are validated, noting the limitations of such a high level of potential error.

CONCLUSION

Pre-test analysis indicated an expected nitrogen liquefaction rate of 0.2 g/s in the tank, while test results revealed that only 0.096 g/s could be achieved. Through thorough review of the system, it is concluded that the HATCHBAC tank incurred higher-than-expected heat leak, resulting in decreased liquefaction efficacy. While the 4.8 W heat leak measured through a boil-off test matches the predictive values, it does not account for bulk heating of the liquid or vapor nitrogen in the tank, leaving much of the heat leak potentially unaccounted for. Due to instrumentation limitations and sensor measurement uncertainty, it is difficult to determine the exact source and amount of heat leak.

From these findings, further testing with added instrumentation would be beneficial to capture the precise source of heat leak. Further heat leak reducing measures should also be taken to improve the efficacy of the HATCHBAC tank for future ISRU applications. In addition, the development of higher capacity

cryocoolers would be beneficial for continued and increased-scale use of HATCHBAC tanks, as both analysis and testing indicated the limiting factor for improvement was heavily reliant on the available cryocooler lift.

REFERENCES

[1] Carney, A., Walker, A., Skaff, T., "Broad Area Cooling with Hybrid Additive Manufactured Pressure Vessel Analysis," 2023 AIAA SciTech Forum, January 2023

[2] Gilmore, David G., "Spacecraft Thermal Control Handbook Volume 1: Fundamental Technologies," Aerospace Press, December 15, 2002

[3] Barron, Randall F., Nellis, Gregory F., "Cryogenic Heat Transfer." Boca Raton, FL. Taylor & Francis Group, 2016

[4] Bergman, Theodore L., Lavine, Adrienne S., Incropera, Frank P., Dewitt, David P., "Fundamentals of Heat and Mass Transfer." Hoboken, NJ. John Wiley & Sons, 2011

[5] D.W Plachta, W.L Johnson, J.R Feller, "Zero Boil Off System Testing", CEC 2015, Wisconsin , WI, June 28 – July 2, 2015

[6] Johnson, Wesley L., Hauser, Daniel M., Platchta, David W., Sutherlin, Steven G., Valenzuelas, Juan G., Smith, James W., Stephen, Jonathan R., "Investigation into Cryogenic Tank Insulation Systems for the Mars Surface Environment," 2018 Joint Propulsion Conference, Cincinnati, OH, July 2018

[7] Hauser, Daniel M., Johnson, Wesley L., Sutherlin, Steven G., "Liquefaction and Storage of In-Situ Oxygen on the Surface of Mars," 8th Symposium Space Resource Utilzation, San Diego, California, AIAA 2016-0721, January 4-8, 2016

[8] Muratov, C.B., Osipov, V.V., Smelyanskiy, V.N. "Issues of Long-Term Cryogenic Propellant Storage in Microgravity." Ames Research Center, 2011, NASA/TM-2011-215988

[9] Ross, R. G. "Quantifying MLI Thermal Conduction in Cryogenic Applications from Experimental Data." 2015 Cryogenic Engineering Conference, Tucson, AZ, June 2015